doi:10.1152/ajpheart.00137.2008.

Intracellular calcium dynamics at the core of endocardial stationary spiral waves in Langendorff-perfused rabbit hearts

Liang Tang,[1] Gyo-Seung Hwang,[1] Hideki Hayashi,[1] Juan Song,[1] Masahiro Ogawa,[1] Kenzaburo Kobayashi,[1] Boyoung Joung,[1] Hrayr S. Karagueuzian,[2] Peng-Sheng Chen,[1] and Shien-Fong Lin[1]

[1]*Krannert Institute of Cardiology, Department of Medicine, Indiana University School of Medicine, Indianapolis, Indiana; and* [2]*Division of Cardiology, Department of Medicine, David Geffen School of Medicine, University of California, Los Angeles, California*

Submitted 7 February 2008; accepted in final form 8 May 2008

Tang L, Hwang GS, Hayashi H, Song J, Ogawa M, Kobayashi K, Joung B, Karagueuzian HS, Chen PS, Lin SF. Intracellular calcium dynamics at the core of endocardial stationary spiral waves in Langendorff-perfused rabbit hearts. *Am J Physiol Heart Circ Physiol* 295: H297–H304, 2008; doi:10.1152/ajpheart.00137.2008.—In vitro models of sustained monomorphic ventricular tachycardia (MVT) are rare and do not usually show spiral reentry on the epicardium. We hypothesized that MVT is associated with the spiral wave in the endocardium and that this stable reentrant propagation is supported by a persistently elevated intracellular calcium (Ca_i) transient at the core of the spiral wave. We performed dual optical mapping of transmembrane potential (V_m) and Ca_i dynamics of the right ventricular (RV) endocardium in Langendorff-perfused rabbit hearts ($n = 12$). Among 64 induced arrhythmias, 55% were sustained MVT (>10 min). Eighty percent of MVT showed stationary spiral waves (>10 cycles, cycle length: 128 ± 14.6 ms) in the endocardial mapped region, anchoring to the anatomic discontinuities. No reentry activity was observed in the epicardium. During reentry, the amplitudes of V_m and Ca_i signals were higher in the periphery and gradually decreased toward the core. At the core, maximal V_m and Ca_i amplitudes were 42.95 ± 5.89% and 43.95 ± 9.46%, respectively, of the control ($P < 0.001$). However, the trough of the V_m and Ca_i signals at the core were higher than those in the periphery, indicating persistent V_m and Ca_i elevations during reentry. BAPTA-AM, a calcium chelator, significantly reduced the maximal Ca_i transient amplitude and prevented sustained MVT and spiral wave formation in the mapped region. These findings indicate that endocardial spiral waves often anchor to anatomic discontinuities causing stable MVT in normal rabbit ventricles. The spiral core is characterized by diminished V_m and Ca_i amplitudes and persistent V_m and Ca_i elevations during reentry.

reentry; endocardial mapping; monomorphic ventricular tachycardia

SPIRAL WAVES have been discovered in different types of excitable media and in biological systems (18, 35). In the heart muscle, spiral waves could result in reentrant excitation of myocardial cells, causing potentially lethal cardiac arrhythmias, including ventricular tachycardia (VT) and ventricular fibrillation (VF) (11, 33). Most previous studies have focused only on the transmembrane potential (V_m) activity of spiral waves (1, 12, 14, 17, 20, 25, 29). It is known that monomorphic VT (MVT) may correspond to a stationary anchored spiral wave, whereas polymorphic VT and VF correspond to a nonstationary (meandering) spiral wave. Nevertheless, the intracellular calcium (Ca_i) dynamics at the core of a stationary spiral wave during MVT remain unclear. Studies have shown that Ca_i dynamics may play an important role in the destabilization of VT due to spiral wave breakup to cause transition from stationary to violently meandering spiral activity (4, 7, 10, 15). Therefore, it is of great interest to better understand Ca_i transient characteristics at the spiral core during sustained MVT.

Earlier experimental and theoretical studies on MVT were performed in real or virtual tissues with a low degree of heterogeneity such as thin slices of epicardial muscles superfused in tissue bath, monolayers of cultured myocytes, or computer simulations (4, 11, 14). The characteristics of a stationary spiral wave in the endocardium with a high degree of heterogeneity are, however, not fully understood. Such paucity of information may be, at least in part, due to the lack of an adequate experimental model of sustained MVT in an isolated heart preparation. It is known that in vitro models of sustained MVT are rare and do not usually show spiral reentry on the epicardium, except when the heart is treated with high doses of L-type calcium channel blocker (36). In this work, we created a sustained MVT model and induced a long-lasting stationary spiral wave in the right ventricular (RV) endocardium of Langendorff-perfused rabbit hearts. We hypothesized that MVT was associated with the spiral wave in the endocardium and that this stable reentrant propagation was supported by a persistently elevated Ca_i transient at the core of the spiral wave. To test this hypothesis, we performed a high-resolution dual V_m and Ca_i optical mapping of the endocardial spiral activity during sustained MVT. This study enabled us not only to directly visualize spiral waves in the endocardium but also to follow the details of their behavior to *1*) study V_m and Ca_i dynamics at the spiral core and *2*) define the anatomic characteristics of the endocardial structures that served to anchor the core of the spiral wave.

MATERIALS AND METHODS

The study protocol was approved by the Institutional Animal Care and Use Committee and followed the guidelines of the American Heart Association.

Surgical preparations. Twelve New Zealand White rabbits (weight: 4–5 kg) of either sex were intravenously injected with 1,000 units of heparin and anesthetized with ketamine (20 mg/kg) and xylazine (5 mg/kg). After a median sternotomy, the whole heart was rapidly

Address for reprint requests and other correspondence: S.-F. Lin, Krannert Institute of Cardiology, Indiana Univ. School of Medicine, 1801 N. Capitol Ave., Rm. E308, Indianapolis, IN 46202 (e-mail: linsf@iupui.edu).

The costs of publication of this article were defrayed in part by the payment of page charges. The article must therefore be hereby marked "*advertisement*" in accordance with 18 U.S.C. Section 1734 solely to indicate this fact.

excised and retrogradely perfused through the ascending aorta with 37°C Tyrode solution [pH 7.3–7.4; composed of (in mM) 125 NaCl, 4.5 KCl, 0.25 $MgCl_2$, 24 $NaHCO_3$, 1.8 NaH_2PO_4, 1.8 $CaCl_2$, and 5.5 glucose] equilibrated with 5% CO_2-95% O_2. The coronary perfusion pressure was regulated between 80 and 95 mmHg. Each isolated heart was allowed to stabilize with perfusion for ~10 min (equilibration period) before the following dissection and mapping protocols.

To expose the RV endocardium, we cut open the right atrial (RA) free wall toward the atrial septum above the right coronary artery (RCA). The RCA was tied off just close to the posterior descending artery to ensure continuous perfusion of the RV free wall without significant leakage. A base-to-apex cut along the posterior descending artery separated the free wall from the septum on one side of the ventricle, forming an RV flap (Fig. 1). This reparation ensured a perfused RV endocardium with normal anatomic structures exposed in the isolated rabbit heart. VT was induced by rapid burst ventricular pacing at cycle lengths of 60–90 ms (5-ms pulse duration for 10–20 s).

High-resolution, dual optical mapping of V_m and Ca_i transients. We used 0.5 mg of Rhod-2 AM (Invitrogen) dissolved in l ml DMSO containing Pluronic F-127 [20% (wt/vol)] to stain the tissue for Ca_i recording. The dissolved Rhod-2 solution (1.48 μM in Tyrode solution) was infused into the heart over a 10-min period. Following that, the heart was perfused with dye-free Tyrode solution for 15 mins for deesterification of Rhod-2 AM. The heart was then stained again by a direct bolus injection of voltage-sensitive dye (RH237, Invitrogen) into the perfusion system. The voltage-sensitive dye RH237 was used because its emission bandpass differs from that of Rhod-2, thereby preventing cross-talk between the two signals (9, 24). The electromechanical uncoupler 2,3-butanedione monoxime (BDM; diacetyl monoxime, Sigma, St. Louis, MO) was added to the perfusate at a concentration of 15 mM to minimize motion artifacts during optical recording.

After an illumination by excitation laser light at 532 nm, the fluorescence from the double-stained heart was collected using two charge-coupled device (CCD) cameras (Dalsa, Waterloo, ON, Canada) covering the same mapped field. We used a grid to calibrate the locations of the field of view of these two CCD cameras so we could compare the recordings of V_m and Ca_i from the same locations. The CCD camera for V_m was fitted with a 715-nm long-pass filter, and the CCD camera for Ca_i was fitted with a 580 ± 20-nm band-pass filter.

We mapped the RV endocardium, acquiring fluorescent signals from 128 × 128 sites (25 × 25 mm^2) simultaneously, resulting in a spatial resolution of 0.2 × 0.2 mm^2/pixel. In six preparations, after confirming the spiral wave anchoring to the RV endocardium during sustained MVT induced by rapid burst pacing, we rotated the heart to map epicardial activities in the LV and RV, both anterior and posterior walls. Simultaneous ECGs from the RA-LV and LV-RV were closely monitored to ensure sustained MVT while rotating the heart for epicardial mapping. It should be noted that the epicardial mapping was performed both before (intact) and after cut-open RV flaps were created. We acquired 1,000 frames continuously at a sampling rate of 260 frames/s, or 3.85 ms/frame. The image acquisition was controlled by a custom-designed program based on LabView and the IMAQ Vision toolset (National Instruments, Austin, TX).

In additional four RV flap preparations of isolated rabbit hearts, BAPTA-AM (20 μM, Sigma), a calcium chelator, was added to the Tyrode perfusate and infused for 60 min to eliminate the calcium elevation effect. The rapid burst pacing protocol was performed before (baseline) and after BAPTA-AM infusion, in an attempt to induce MVT.

Data analysis. Rotating spiral waves were identified by examination of all videos, and sustained MVT episodes (over 10 min) were identified by simultaneous ECG recordings. Spiral waves were considered stationary when the tip of the spiral, which circulated around the core, followed a closed circular or elliptical trajectory and the periodicity was preserved everywhere outside the core. The location, cycle length, and dimensions of the spiral core were determined by tracing the trajectory of the tips of the wave propagation. Because two CCD cameras were used, the same anatomic location may appear at different coordinates on V_m and Ca_i maps. Therefore, we implanted four cactus needles on the endocardium as registration markers. A software program then used these markers to match the pixels on V_m and Ca_i maps to the same locations in the mapped region. Data analyses were performed only with aligned maps.

Data are presented as means ± SD. Student's *t*-test was used to test for statistical differences. The null hypothesis was rejected at a value of $P < 0.05$.

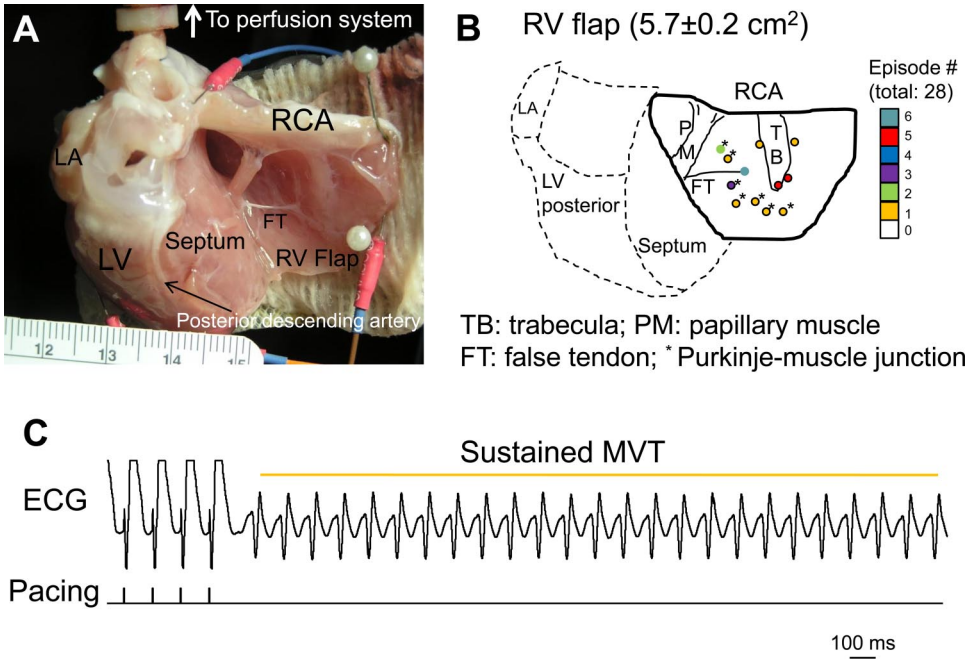

Fig. 1. Cut-open right ventricular (RV) flap preparation in isolated rabbit hearts. *A*: anatomy of the RV endocardium. FT, false tendon; RCA, right coronary artery; LA, left atrium; LV, left ventricle. See text for surgical details. *B*: schematic diagram of the RV flap structure and spatial distribution of spiral core anchoring in the endocardium. The color bar indicates the count of episodes showing the core anchored around the specific area. TB, trabeculae; PM, papillary muscle. *C*: typical ECG recording of induced sustained monomorphic ventricular tachycardia (MVT) by rapid burst pacing in this preparation.

RESULTS

Of 64 arrhythmias induced in the RV endocardium, 55% were sustained MVT (over 10 min; Fig. 1*C*); 34% as VF and 11% for polymorphic VT. Among MVTs, 28 of 35 episodes showed stationary spiral waves (>10 cycles, cycle length: 128 ± 14.6 ms) in the mapped region, whereas the remaining episodes (20%) showed regular planar wave front propagation, probably part of bigger reentrant circuits in the heart with the core anchoring outside of the mapped area. Table 1 shows the distribution of the 35 MVT and 28 spiral waves among the 12 isolated rabbit hearts studied. Clockwise and counterclockwise wave front rotations were evenly distributed.

V_m and Ca_i at the core of the stationary spiral wave. Figure 2*A* shows a series of video frames of Ca_i signals and V_m isochronal maps obtained during a complete cycle of a clockwise rotating spiral wave in the setting of MVT. The spiral activity was recorded in the RV endocardium (Fig. 2*B*). The start of the spiral cycle was timed at 0 ms and the cycle length was 128 ms, which was almost same as that of MVT, as shown in the simultaneous ECG recording (Fig. 2*E*). The curvature of the wave tips increased toward the center of the rotation (i.e., core area; Fig. 2*A*) and resulted in a characteristic spiral-like shape. The corresponding V_m isochronal map also showed a spiral-like reentrant wave front propagation.

Figure 2*C* shows the patterns of local V_m and Ca_i signals obtained from selected points (*points a–f*) along a line that crossed the core region during the spiral wave propagation. The amplitude of the V_m signal (differences between the peak and trough) was higher in the periphery and gradually decreased toward the center of the core. V_m signals also showed that the core region failed to repolarize fully and lacked clear diastolic activity during reentry. Accordingly, the amplitude of the Ca_i signal was diminished toward the core. At the core, the peak of the Ca_i signal was 29 ± 2.65% lower than that of surrounding tissues. The trough of the Ca_i signal was, however, 26 ± 8.55% higher than the trough of the Ca_i signal in the periphery, indicating a persistent Ca_i elevation (Ca_i at the midlevel between systolic and diastolic) at the core during reentry. The superimposed traces (not shown) illustrated that the Ca_i transient closely tracked the V_m activity after a delay of 34.65 ± 18.23 ms at the myocardial tissues surrounding the core. However, due to the diminished V_m and Ca_i amplitude at the core (Fig. 2*C*, *trace c*), it was difficult to determine if V_m and Ca_i dynamics tracked each other. At the edge of the core region (Fig. 2*C*, *trace d*), calcium alternans was found to be present. In addition, a very large difference was apparent in V_m and Ca_i signal peaks occurring at either side of the core. For example, at the vertical red lines in Fig. 2*C*, V_m and Ca_i signals at *traces a* and *b* were near the bottom, indicating that V_m was fully repolarized and the Ca_i transient returned to the diastolic level. At this time, V_m and Ca_i signals in Fig. 2*C*, *traces e* and *f*, were at peak. Although there were local differences in the Ca_i activation pattern, the temporal pattern was uniform throughout the recording. Accordingly, the ECG showed stable monomorphic activity, which lasted over 10 min (Fig. 2*E*). Upon termination of the spiral wave, V_m and Ca_i signals at all points including those in the core region returned to the diastolic level (data not shown).

Table 1. *Summary of MVT induction and associated stationary spiral activity in the mapped region (right ventricular endocardium) in 12 isolated rabbit hearts*

	MVT Episodes	Stationary Spiral Episodes	Planar Wave Propagation Episodes
Experiment 1	3	3	
Experiment 2	2	2	
Experiment 3	1		1
Experiment 4	5	4	1
Experiment 5	5	3	2
Experiment 6	1	1	
Experiment 7	3	3	
Experiment 8	2	2	
Experiment 9	4	3	1
Experiment 10	3	2	1
Experiment 11	4	3	1
Experiment 12	2	2	
Total	35	28	7

MVT, monomorphic ventricular tachycardia.

Figure 3*A* shows representative examples of V_m and Ca_i signals at the core and those of surrounding tissues at either side (P1 and P2). The core was characterized by a significantly decreased V_m amplitude, consistent with another report (11) in epicardial tissues. Presumably, the voltage-sensitive fluorescent signal is linear with V_m. The diastolic trough of the V_m signal was defined as 0%, whereas the systolic peak of the V_m signal was 100%. The maximal V_m amplitude at the core was determined to be 42.95 ± 5.89% of the V_m amplitude when the same site supported a planar propagating wavefront. The corresponding maximal Ca_i amplitude at the core was 43.95 ± 9.46% normalized to that of the surrounding tissues ($P < 0.001$; Fig. 3*B*). Note that both V_m and Ca_i signals at the core never reached baseline levels, indicating partially repolarization and persistent Ca_i elevation in the core region during reentry. The dashed blue line in Fig. 3*A* represents superimposed V_m and Ca_i traces, showing that at the surrounding tissues outside of the core, Ca_i transients closely tracked V_m activities during reentry. Such a close Ca_i and V_m tracking relationship was, however, less obvious at the core. Further investigation is required to elucidate the Ca_i/V_m tracking relationship and underlying mechanism at the core.

To determine whether the low V_m and Ca_i amplitudes at the core resulted from anatomic discontinuities or were functionally based, we compared the V_m and Ca_i map during spiral wave activity and during planar wave propagation in the same hearts shown in Fig. 2*D*. The same V_m and Ca_i signals during the planar wave propagation were also recorded during reentry when these same sites became located at the very core of the reentry. A considerable decrease in the amplitudes of both V_m and Ca_i signals was observed (Fig. 2*C*). Indeed, although the region contained an anatomic discontinuity (in this case, the endocardial trabecula ridge), during planar propagation, V_m and Ca_i activities were uniform and high (i.e., normal amplitude) throughout the segment. These reproducible findings indicate that the observed differences in the fluorescence associated with the spiral wave activity reflect the functional electrophysiological differences between the core and the surrounding areas.

Stationary spiral wave core anchoring. All the 28 episodes of stationary spiral wave during MVT showed anchoring of the core to an obvious anatomic discontinuity in the RV endocardium, such as trabecula, false tendon insertion from papillary

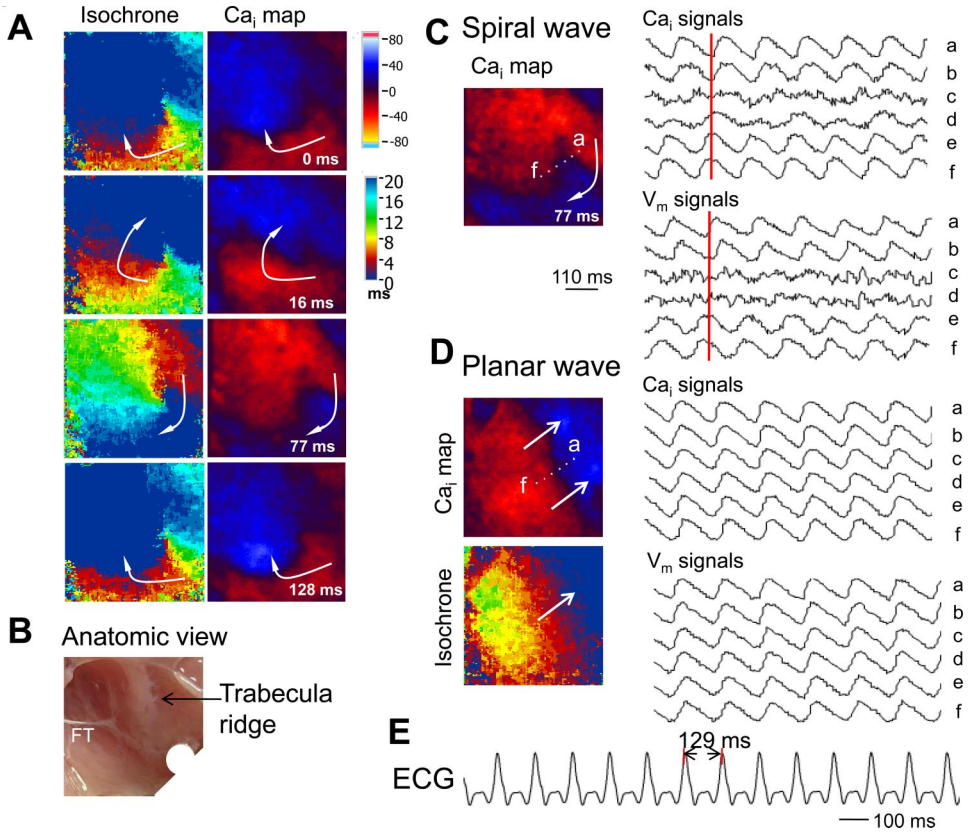

Fig. 2. *A*: sequence of video frames of one complete cycle of a clockwise rotating intracellular calcium (Ca_i) spiral wave and the corresponding transmembrane potential (V_m) isochronal maps in the RV endocardium of the isolated rabbit heart preparation. The spiral wave lasted >10 cycles (cycle length: 128 ms) during sustained MVT. The white arrows indicate the direction of the reentrant wave propagation. The Ca_i map is timed 0 ms at the start of the cycle. *B*: anatomic view of the endocardial mapped region. *C* and *D*: V_m and Ca_i signals at selected points (*points a–f*) along a line across the core during the spiral wave (*C*) and planar wave propagation in the mapped region (*D*). The white arrows indicate the direction of the wave propagation. *Traces a–f* show signals along *points a–f*. *E*: simultaneous ECG recording. MVT cycle length: 129 ms.

muscle to the myocardium (false tendon insertion), and discrete Purkinje-muscle junction (PMJ). No spiral activities were observed during the optical mapping of the epicardial tissues of the LV and RV, both anterior and posterior, before (intact) and after cut-open preparations. Figure 1*B* shows the spatial distribution of the spiral core location in the RV endocardium. The color bar in Fig. 1*B* represents the number of episodes showing the core attached to a particular endocardial myocardium

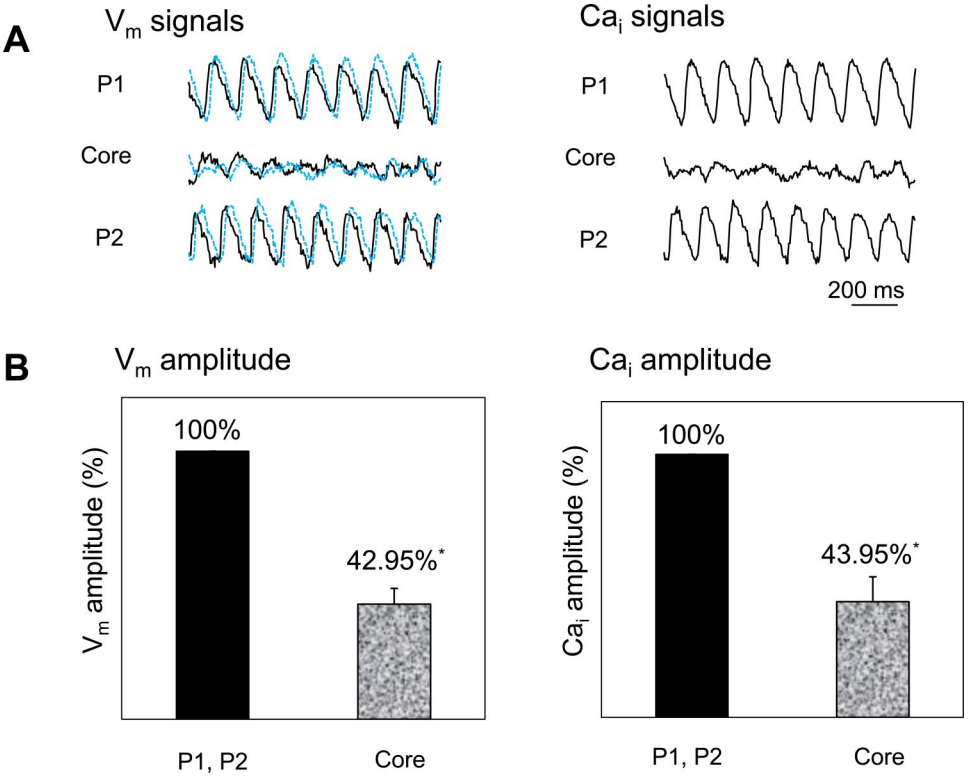

Fig. 3. *A*: typical V_m and Ca_i signals at the spiral core during reentry. The V_m traces were superimposed by the Ca_i signals (dashed blue traces). P1, periphery tissue around the core at one side; P2, periphery tissue around the core at the other side. *B*: maximal V_m and Ca_i amplitudes (signal differences between the peak and trough) at the core normalized to the surrounding tissues (P1 and P2). $^*P < 0.001$.

shown in the schematic diagram. Approximately 43% (12 of 28) stationary spiral waves were found to anchor around the endocardial trabecula. The anatomy also shows a false tendon insertion to the endocardial ventricular muscle. The insertion acted as an anatomic obstacle, and ~21% of spiral waves (6 episodes) anchored to that specific area. Careful examination of the anatomic structures found that, altogether, the core anchoring to the discrete PMJ in the lower and left areas of the RV endocardium accounted for the remaining 36% episodes. The result showed that the spiral core was more likely to anchor around an anatomic obstacle with a larger size. The dimensions of the endocardial trabecula ridge, false tendon insertion, and PMJ were measured at 6.5 ± 2.2, 0.87 ± 0.2, 0.25 ± 0.2 mm^2, respectively ($P < 0.001$; Fig. 4).

There was a positive correlation between the spiral core size and the associated anatomic obstacle size in the endocardium ($r = 0.98$; Fig. 4). Phase-plane analysis was performed on reentry data to determine the instantaneous location of the reentry core, indicated by the phase singularity point (6). The locations of phase singularities from every frame during one complete reentry were traced to determine the core area (Fig. 4*A*). Corresponding to the anatomic obstacle sizes, the core sizes anchored around the trabecula ridge (Fig. 4*A*, *region a*), false tendon insertion (Fig. 4*A*, *region b*), and PMJ (Fig. 4*A*, *region c*) were 10.4 ± 3.9, 4.6 ± 1.6, 2.3 ± 0.9 mm^2, respectively ($P < 0.02$). These results indicate that the size of the spiral core is mainly determined by the size of the anatomic obstacle to which the spiral core anchors.

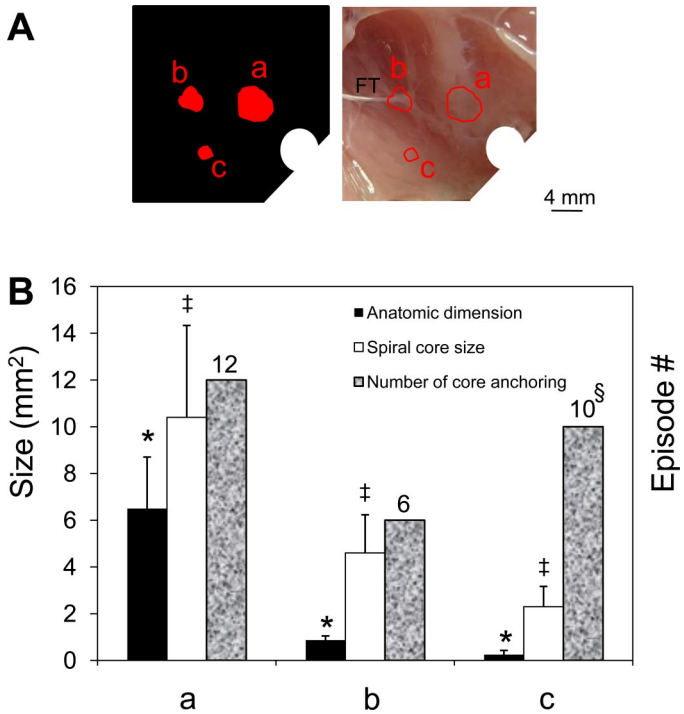

Fig. 4. *A*: Shape and dimension of the spiral cores anchoring around endocardial trabecula ridge (*region a*), FT insertion (*region b*), and PMJ (*region c*) as shown in the phase singularity map during one complete reentrant cycle. *B*: correlation between the anatomic obstacle size, incidence of anchoring (number of episodes), and the associated spiral wave core size ($r = 0.98$). *$P < 0.001$; ‡$P < 0.02$. §Total number of episodes of the spiral wave anchored to a discrete PMJ site in the mapped region of the RV endocardium.

Effect of BAPTA-AM on MVT. After confirming the spiral wave activity in the mapped region of the RV endocardium during sustained MVT, we perfused four isolated rabbit hearts with BAPTA-AM, a calcium chelator (28). BAPTA-AM is known to incorporate into tissues slowly (5, 22); therefore, we perfused BAPTA-AM for 60 min and then attempted to induce MVT again by rapid burst pacing. Figure 5 shows that BAPTA-AM significantly reduced the maximal Ca_i amplitude in the mapped region (34.6 ± 3.6% of the control, $P < 0.001$), whereas the voltage signal (V_m) was almost unchanged. In contrast to sustained VT at baseline, after drug treatment, VT lasted 5.88 ± 2.41 s with spontaneous termination. About 10% of the MVT episodes lasted ~25 s before termination, as shown in the ECG recording in Fig. 5*C*. No associated spiral wave activity was observed in the mapped region after BAPTA-AM. In addition, BAPTA-AM increased the VT cycle length from 138.5 ± 8.4 ms at baseline to 184.5 ± 8.7 ms ($P < 0.001$; Fig. 5*D*).

DISCUSSION

Langendorff-perfused rabbit heart with sustained MVT model. It has been known that sustained MVT occurs only in a very small number of Langendorff-perfused rabbit heart preparations (13). However, our endocardial model showed a 55% MVT induction by rapid burst pacing. The high induction rate could be attributed, at least in part, to the cut-open RV flap preparation, which reduces the tissue mass available for fibrillation and decreases the number of wavefronts interfering with the reentrant wave for breakup. Kim et al. (16) demonstrated that a decrease in the number of wavefronts in VF by tissue mass reduction in isolated swine RV preparations caused a transition from chaotic to periodic (VT) dynamics. In this study, the application of the electromechanical uncoupler BDM may also have contributed to the MVT induction. It was reported that BDM shortened the action potential duration (APD) measured to 90% repolarization and reduced the slope of the APD restitution curve in isolated swine RV tissues (19, 26). As a result, BDM prevented the induction of VF and converted existing VF into a stable periodic rhythm.

Endocardial trabecula, false tendon insertion, and PMJ as reentry anchoring sites. Previous experimental and computer simulation studies of V_m activity during reentry have demonstrated the role of papillary muscle as a spiral wave anchoring site that stabilized wave conduction in the isolated swine RV in the setting of VT and VF (17, 29). A consistent and important finding in our study is that naturally occurring anatomic obstacles, the false tendon insertion, trabecula, and PMJ, are apparently large enough obstacles to anchor wavefront propagation during reentry. Bundles of Purkinje fibers were found in the endocardial trabecula and papillary muscle root at the reentry site by histological examination of isolated swine RV tissues (30). Hence, it is clear that the chances for reentry anchoring are higher for the PMJ compared with intact myocardial tissue, which could be attributable to the unique intrinsic ionic properties causing a reduced repolarization reserve in Purkinje fibers and the junctional tissue (21). Whereas myocardial cells are tightly coupled electrically to one another, Purkinje fibers are relatively insulated from the myocardium, thereby reducing the electrotonic sink that they encounter. This results in a greater modulation of membrane potential by a

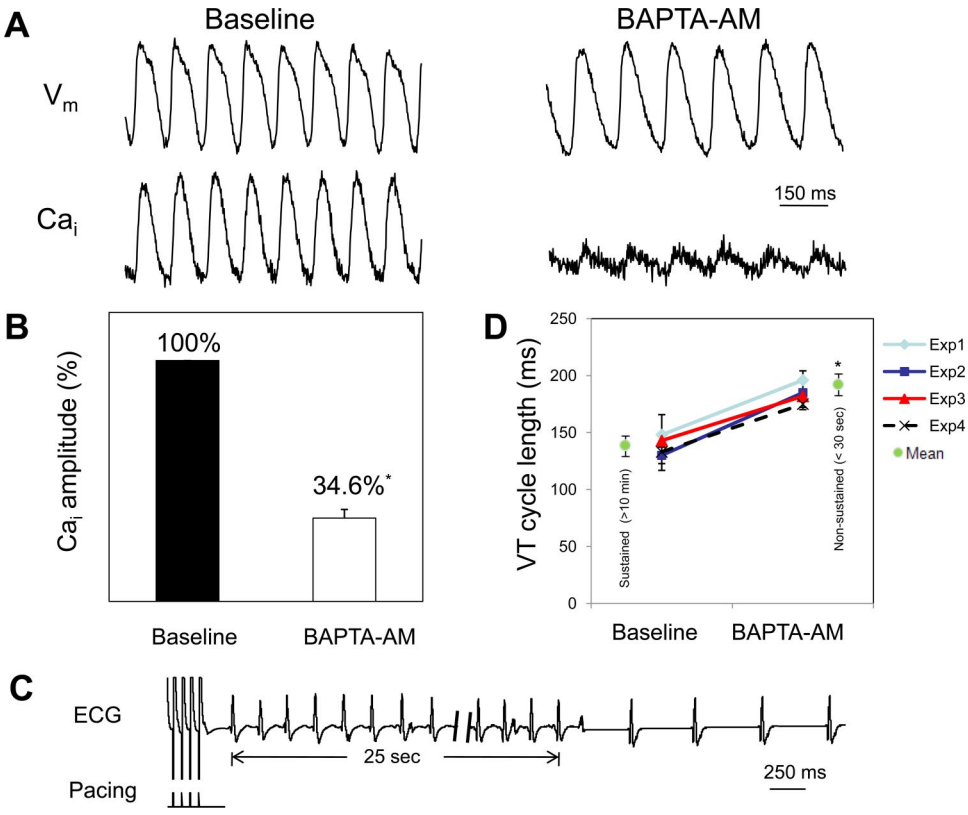

Fig. 5. *A*: V_m and Ca_i signal recordings of the same pixel at baseline and 60 min after BAPTA-AM perfusion (20 μM). *B*: BAPTA-AM significantly reduced maximal Ca_i amplitudes. *C*: ECG recordings of nonsustained MVT (spontaneous termination within 30 s) after BAPTA-AM treatment. *D*: comparison of induced VT cycle lengths at baseline and after BAPTA-AM. Exp1–Exp4, *experiments 1–4*. $*P < 0.001$.

given amount of current, allowing reentry to form more readily. Moreover, the trabecula ridge and false tendon insertion, which create a sudden increase of muscle thickness, increase the current sink for the incoming wavefront. As a result, conduction block occurs at the site of source-sink mismatch, resulting in the formation of reentry.

MVT associated with endocardial spiral waves. Valderrábano et al. (30) demonstrated that reentry in the isolated swine RV preparation was mostly transmural and required the participation of subendocardial structures such as the papillary muscle and trabecula. In the present study, we observed that endocardial spiral waves anchoring around the false tendon insertion, trabecula, and PMJ were found in the majority of sustained MVT in normal rabbit ventricles. In comparison, no spiral waves were observed in the epicardial tissues of the isolated hearts during MVT, confirming the importance of the anatomic discontinuities and the association of MVT with spiral wave activity on the endocardial surfaces. The results are consistent with previous findings that ventricular arrhythmia may originate from the Purkinje network and PMJ in the endocardium with a breakthrough activity to the epicardium (2, 8, 27).

Ca_i dynamics at the stationary spiral core during MVT. We found a persistent elevation of the Ca_i level at the core during reentry (Fig. 3), which might help maintain the reentry anchoring. It is well known that Ca_i determines the shape of V_m and the APD through various calcium ionic channels, such as the L-type calcium channel, the sodium/calcium exchanger (NCX), and calcium nonselective channels (3, 9, 32). The elevated Ca_i levels are restored during repolarization by the rapid reuptake of Ca_i into the sarcoplasmic reticulum. However, an elevated Ca_i level at the reentrant core could activate the electrogenic NCX, which in turn generates a net depolarizing inward current and help maintain a prolonged APD at the core. In this context, the elevated Ca_i at the core might be required to help maintain the reentry. Given the bidirectional coupling between V_m and Ca_i (34), our present study suggests that both V_m and Ca_i might be important in determining the spiral wave dynamics on the rabbit endocardium, which is supported by our observations that both V_m and Ca_i are elevated at the spiral core during reentry (Fig. 3*A*).

Our results are consistent with the observation of Warren et al. (31) that simultaneous elevation of V_m and Ca_i are present in the vicinity of the nonstationary core during VF in blood-perfused pig hearts. They also reported that the application of BAPTA-AM for 10–15 min did not reduce the incidence of wavebreaks during VF. Such an ineffectiveness of BAPTA-AM treatment in altering VF dynamics might be due to the relative short duration of drug perfusion (22). In the present study, infusion of BAPTA-AM over a 60-min period significantly reduced the Ca_i level, preventing sustained MVT and spiral wave formation in the mapped region. Recently, it has been shown that BAPTA-AM converted VF to VT induction after 70 min of perfusion in intact rabbit hearts (22). Using the cut-open RV flap preparation in isolated rabbit hearts, we observed the conversion of sustained VT induction to nonsustained VT after drug treatment. These results suggest the importance of lowering Ca_i elevation and confirm the antiarrhythmic effect of BAPTA-AM (5).

We also found that, similar to a previous study (23), Ca_i dynamics during VT closely tracked V_m activities at the surrounding tissues (Fig. 3). Omichi et al. (23) first reported the different relationship between Ca_i and V_m during VT and VF in the isolated swine RV preparation. Warren et al. (31) then

reported the dissociation between Ca_i and V_m during VF and its possible role in VF maintenance. Their results showed that Ca_i waves usually bore no relationship to membrane potential waves during the nonreentrant fractionated waves typical of VF, whereas they tracked each other closely during VT and complete reentrant cycles during VF. Our results provide further evidence that, except at the core, Ca_i dynamics track V_m signals during stable reentry.

Study limitations. The BAPTA-AM infusion significantly reduced Ca_i signals, preventing sustained MVT and spiral wave formation in the mapped region. One possible limitation of the study is that BAPTA-AM could be influencing refractoriness, which could also affect the dynamics of VT and spiral core. Further studies are required to determine if the spiral core is solely caused by Ca_i elevation. In addition, due to the diminished amplitudes at the spiral core, it was difficult to conclusively determine whether V_m and Ca_i signals at the spiral core are associated or dissociated with each other.

Clinical implications. MVT is often associated with stationary spiral wave anchoring to a structural heterogeneity. The anchoring of the spiral core was demonstrated to be anatomic obstacles, and the incidence of anchoring increased with obstacle size. Endocardial trabecula and false tendon insertion from the papillary muscle may be targets for ablative procedures in humans to prevent VT recurrences. Furthermore, persistently elevated Ca_i at the core could play an important role in the dynamics of spiral wave activity. Further elucidation of the relationships between abnormal Ca_i dynamics and spiral waves may potentially improve the clinical efficacy of antiarrhythmic drugs.

ACKNOWLEDGMENTS

We thank Avile McCullen and Lei Lin for the technical assistance.

GRANTS

This work was supported in part by National Heart, Lung, and Blood Institute Grants P01-HL-78931, R01-HL-78932, R01-HL-58533, R01-HL-66389, and R01-HL-71140, by American Heart Association Established Investigator Award 0540093N, and by the Laubisch Endowment of the University of California (Los Angeles, CA).

REFERENCES

1. **Beaumont J, Davidenko N, Davidenko JM, Jalife J.** Spiral waves in two-dimensional models of ventricular muscle: formation of a stationary core. *Biophys J* 75: 1–14, 1998.
2. **Berenfeld O, Jalife J.** Purkinje-muscle reentry as a mechanism of polymorphic ventricular arrhythmias in a 3-dimensional model of the ventricles. *Circ Res* 82: 1063–1077, 1998.
3. **Bers DM.** Calcium fluxes involved in control of cardiac myocyte contraction. *Circ Res* 87: 275–281, 2000.
4. **Bien H, Yin L, Entcheva E.** Calcium instabilities in mammalian cardiomyocyte networks. *Biophys J* 90: 2628–2640, 2006.
5. **Billman GE.** Intracellular calcium chelator, BAPTA-AM, prevents cocaine-induced ventricular fibrillation. *Am J Physiol Heart Circ Physiol* 265: H1529–H1535, 1993.
6. **Bray MA, Lin SF, Aliev RR, Roth BJ, Wikswo JP Jr.** Experimental and theoretical analysis of phase singularity dynamics in cardiac tissue. *J Cardiovasc Electrophysiol* 12: 716–722, 2001.
7. **Cagalinec M, Chorvat D Jr, Mateasik A, Bacharova L.** Sustained spiral calcium wave patterns in rat ventricular myocytes. *J Cell Mol Med* 11: 598–599, 2007.
8. **Cerrone M, Noujaim SF, Tolkacheva EG, Talkachou A, O'Connell R, Berenfeld O, Anumonwo J, Pandit SV, Vikstrom K, Napolitano C, Priori SG, Jalife J.** Arrhythmogenic mechanisms in a mouse model of catecholaminergic polymorphic ventricular tachycardia. *Circ Res* 101: 1039–1048, 2007.
9. **Choi BR, Salama G.** Simultaneous maps of optical action potentials and calcium transients in guinea-pig hearts: mechanisms underlying concordant alternans. *J Physiol* 529: 171–188, 2000.
10. **Chudin E, Goldhaber J, Garfinkel A, Weiss J, Kogan B.** Intracellular Ca^{2+} dynamics and the stability of ventricular tachycardia. *Biophys J* 77: 2930–2941, 1999.
11. **Davidenko JM, Pertsov AV, Salomonsz R, Baxter W, Jalife J.** Stationary and drifting spiral waves of excitation in isolated cardiac muscle. *Nature* 355: 349–351, 1992.
12. **Entcheva E, Lu SN, Troppman RH, Sharma V, Tung L.** Contact fluorescence imaging of reentry in monolayers of cultured neonatal rat ventricular myocytes. *J Cardiovasc Electrophysiol* 11: 665–676, 2000.
13. **Gray RA, Jalife J, Panfilov A, Baxter WT, Cabo C, Davidenko JM, Pertsov AM.** Nonstationary vortexlike reentrant activity as mechanism of polymorphic ventricular tachycardia in the isolated rabbit heart. *Circulation* 91: 2454–2469, 1995.
14. **Huffaker RB, Weiss JN, Kogan B.** Effects of early afterdepolarizations on reentry in cardiac tissue: a simulation study. *Am J Physiol Heart Circ Physiol* 292: H3089–H3102, 2007.
15. **Ishida H, Genka C, Hirota Y, Nakazawa H, Barry WH.** Formation of planar and spiral Ca^{2+} waves in isolated cardiac myocytes. *Biophys J* 77: 2114–2122, 1999.
16. **Kim YH, Garfinkel A, Ikeda T, Wu TJ, Athill CA, Weiss JN, Karagueuzian HS, Chen PS.** Spatiotemporal complexity of ventricular fibrillation revealed by tissue mass reduction in isolated swine right ventricle. Further evidence for the quasiperiodic route to chaos hypothesis. *J Clin Invest* 100: 2486–2500, 1997.
17. **Kim YH, Xie F, Yashima M, Wu TJ, Valderrábano M, Lee MH, Ohara T, Voroshilovsky O, Doshi RN, Fishbein MC, Qu Z, Garfinkel A, Weiss JN, Karagueuzian HS, Chen PS.** Role of papillary muscle in the generation and maintenance of reentry during ventricular tachycardia and fibrillation in isolated swine right ventricle. *Circulation* 100: 1450–1459, 1999.
18. **Lechleiter J, Girard S, Peralta E, Clapham D.** Spiral calcium wave propagation and annihilation in *Xenopus laevis* oocytes. *Science* 252: 123–126, 1991.
19. **Lee MH, Lin SF, Ohara T, Omichi C, Okuyama Y, Chudin E, Garfinkel A, Weiss JN, Karagueuzian HS, Chen PS.** Effects of diacetyl monoxime and cytochalasin D on ventricular fibrillation in swine right ventricles. *Am J Physiol Heart Circ Physiol* 280: H2689–H2696, 2001.
20. **Lim ZY, Maskara B, Aguel F, Emokpae R Jr, Tung L.** Spiral wave attachment to millimeter-sized obstacles. *Circulation* 114: 2113–2121, 2006.
21. **Morley GE, Danik SB, Bernstein S, Sun Y, Rosner G, Gutstein DE, Fishman GI.** Reduced intercellular coupling leads to paradoxical propagation across the Purkinje-ventricular junction and aberrant myocardial activation. *Proc Natl Acad Sci USA* 102: 4126–4129, 2005.
22. **Ogawa M, Lin SF, Weiss JN, Chen PS.** Calcium dynamics and ventricular fibrillation. *Circ Res* 102: e52, 2008.
23. **Omichi C, Lamp ST, Lin SF, Yang J, Baher A, Zhou S, Attin M, Lee MH, Karagueuzian HS, Kogan B, Qu Z, Garfinkel A, Chen PS, Weiss JN.** Intracellular Ca dynamics in ventricular fibrillation. *Am J Physiol Heart Circ Physiol* 286: H1836–H1844, 2004.
24. **Qian YW, Clusin WT, Lin SF, Han J, Sung RJ.** Spatial heterogeneity of calcium transient alternans during the early phase of myocardial ischemia in the blood-perfused rabbit heart. *Circulation* 104: 2082–2087, 2001.
25. **Qu Z, Xie F, Garfinkel A, Weiss JN.** Origins of spiral wave meander and breakup in a two-dimensional cardiac tissue model. *Ann Biomed Eng* 28: 755–771, 2000.
26. **Riccio ML, Koller ML, Gilmour RFJ.** Electrical restitution and spatiotemporal organization during ventricular fibrillation. *Circ Res* 84: 955–963, 1999.
27. **Tabereaux PB, Walcott GP, Rogers JM, Kim J, Dosdall DJ, Robertson PG, Killingsworth CR, Smith WM, Ideker RE.** Activation patterns of Purkinje fibers during long-duration ventricular fibrillation in an isolated canine heart model. *Circulation* 116: 1113–1119, 2007.
28. **Tsien RY.** A non-disruptive technique for loading calcium buffers and indicators into cells. *Nature* 290: 527–528, 1981.
29. **Valderrábano M, Kim YH, Yashima M, Wu TJ, Karagueuzian HS, Chen PS.** Obstacle-induced transition from ventricular fibrillation to tachycardia in isolated swine right ventricles: insights into the transition dynamics and implications for the critical mass. *J Am Coll Cardiol* 36: 2000–2008, 2000.

30. **Valderrábano M, Lee MH, Ohara T, Lai AC, Fishbein MC, Lin SF, Karagueuzian HS, Chen PS.** Dynamics of intramural and transmural reentry during ventricular fibrillation in isolated swine ventricles. *Circ Res* 88: 839–848, 2001.
31. **Warren M, Huizar JF, Shvedko AG, Zaitsev AV.** Spatiotemporal relationship between intracellular Ca^{2+} dynamics and wave fragmentation during ventricular fibrillation in isolated blood-perfused pig hearts. *Circ Res* 101: e90–e101, 2007.
32. **Weiss JN.** Ion channels in cardiac muscle. In: *The Mammalian Myocardium*, edited by Langer GA. San Diego, CA: Academic, 1997.
33. **Weiss JN, Garfinkel A, Karagueuzian HS, Qu Z, Chen PS.** Chaos and the transition to ventricular fibrillation: a new approach to antiarrhythmic drug evaluation. *Circulation* 99: 2819–2826, 1999.
34. **Weiss JN, Karma A, Shiferaw Y, Chen PS, Garfinkel A, Qu Z.** From pulsus to pulseless: the saga of cardiac alternans. *Circ Res* 98: 1244–1253, 2006.
35. **Winfree AT.** Spiral waves of chemical activity. *Science* 175: 634–636, 1972.
36. **Wu TJ, Bray MA, Ting CT, Lin SF.** Stable bound pair of spiral waves in rabbit ventricles. *J Cardiovasc Electrophysiol* 13: 414, 2002.